Modelling vibrations of a moderate amplitude in piezoelectric nanoplates using nonlocal elasticity and G/XFEM

Oscar A.G. Suarez[1], Tiago dos Santos[2], Rodrigo Rossi[1]

[1]*Departamento de Engenharia Mecânica, Universidade Federal do Rio Grande do Sul*
Rua Sarmento Leite, 425, Porto Alegre, RS, 90046-902, Brazil.
oagsuarez@ufrgs.br, rrossi@ufrgs.br
[2]*Departamento de Engenharia Mecânica, Universidade Federal de Santa Maria*
Av. Roraima, 1000, Prédio 7, Santa Maria, RS, 97105-900, Brazil
tiago.santos@ufsm.br

Abstract. In this paper, we address the problem of free and unforced vibration of nanoplates immersed in a transverse electric field using the theory of non-local elasticity. The numerical model was obtained using the first-order plate kinematic theory, which included the shear deformation (FSDT) and the approximation spaces in accordance with the homogeneous "p" version of the G/XFEM method with regularity $C^k, k = 2, 4$. The scale effect is approached using the non-local elasticity theory, and moderate amplitude waves are taken into consideration using the von Karmann geometric non-linearity. In this study an electric stationary field is obtained from a potential function that satisfies Maxwell's law for moving current and the electric potential boundary conditions on the free surface of the plate. Investigations on the estimation of the first nonlinear frequency, as well as the stiffness-softening and stiffness-hardening phenomena, are carried out for a simply supported nanoplate. The findings for the proposed numerical models are contrasted with those attained using Lagrange C^0 finite elements, a semi-analytical solution attained using Navier biharmonic modes, and results acquired using the Generalized Differential Quadrature Method (GDQM) from published results. The GFEM approximation space demonstrated its ability to describe all features of the problem at hand.

Keywords: G/XFEM, FSDT nanoplate, vibration, nonlocal elasticity, piezoelectric.

1 Introduction

Recent research on nanostructures with piezoelectric properties has gained centrality in the last decade due to the growing interest of application in NEMS (Nanoelectromechanical Systems) as resonators, nanomotors and nanogenerators, see He et al. [1], Wang [2], Galan et al. [3], and Xu and Wang [4] among others. This is because the physical properties at the nanoscale size, such as thermal and electrical conductivity, outperform those of the material at the macroscale, see Caglar et al. [5] and Huang et al. [6]. In this context, the dynamic behavior of nanostructures has gained prominence in the technical and scientific communities, inspiring an extensive number of investigations in this field. Recently, in addition to the classic approaches to nanoscale problems, which use models such as Molecular Dynamics (MD) (see Belytschko et al. [7], Chowdhury and Okabe [8], and Galashev and Rakhmanova [9]), very accurate, but also very time consuming from the computational point of view, mathematical models using the principles of continuum mechanics have been used.

Regarding the continuum mechanics approach, some proposals have shown approximate satisfactory results in relation to MD, such as the continuum mechanics micromorphic theory (PCMT), Eringen [10], and the nonlocal elasticity theory (NET), Eringen [11]. Many studies have recently been conducted using nonlocal elasticity theory to address free vibration and buckling issues in piezoelectric nanoplates subjected to a thermal gradient and embedded in a transversal electric field. Some of these recent studies are cited in Liu et al. [12] to approach the free vibrations problem with large deflection in piezoelectric nanoplates under the action of the electric field. In Zeng et al. [13], the authors carried out a study accounting for the flexoelectric effect in the nonlinear vibration of the functional graded piezoelectric nanoplates. In Asemi et al. [14] the authors study the application of the non-

linear vibration in piezoelectric nanoplates to approach a nano-electromechanical resonator. The work of Su et al. [15] address the issues of electro-mechanical vibration in functionally graded nanoplates with general boundary conditions. These are just a few examples of works in this field, among a large number of articles that could be mentioned here.

In this study, the authors address the issue of piezoelectric nanoplate's nonlinear vibration in a transverse electric field. The numerical model is obtained by using first order shear deformation theory (FSDT) (see Reddy [16]) and the NET of Eringen [11]. The approximation spaces with regularity $C^k, k = 2, 4$ are obtained by the homogeneous "p" version of the G/XFEM as in de Suarez and Rossi [17] and the transverse electric field follows the same potential function as used in Sladek et al. [18]. The GFEM approxaimation space's performance is evaluated by comparing the findings to those obtained using the FEM-Lagrange C^0 and the semi-analytical solution obtained using the Navier Bi-harmonics modes. In addition, results based on classical elasticity are obtained and compared to previous research. The approximations spaces' capacity to describe stiffness-softening, induced by a rise in the nanoscale coefficient, and stiffness-hardening phenomena, produced by an increase in the electric field, is also investigated .

2 Galerkin finite element formulation

The matrix form of the eigenvalues problem associated with the Galerkin finite element method applied to nonlinear vibrations of a piezoelectric nanoplate subject to a transverse electric field, see Fig. 1, can be written as:

$$\left[\boldsymbol{K} + \boldsymbol{K}_{\mu} + \boldsymbol{K}_{NL}(\boldsymbol{U}) - \omega^2 \left(\boldsymbol{M}_L + \boldsymbol{M}_{\mu}\right)\right] \boldsymbol{U} = \boldsymbol{0} \tag{1}$$

where $\boldsymbol{K}$, $\boldsymbol{K}_{\mu}$, and $\boldsymbol{K}_{NL}$ are the linear, the nonlocal, and the nonlinear stiffness matrices whereas $\boldsymbol{M}$ and $\boldsymbol{M}_{\mu}$ are the linear and nonlocal mass matrices, respectively. In this equation

$$\begin{aligned}\boldsymbol{K} = \sum_{e=1}^{Ne} \Bigg(& \int_{A_e} \boldsymbol{B}_e^{(0)T} \boldsymbol{A} \boldsymbol{B}_e^{(0)} \mathrm{d}A + \int_{A_e} \boldsymbol{B}_e^{(1)T} \boldsymbol{D} \boldsymbol{B}_e^{(1)} \mathrm{d}A - \int_{A} \boldsymbol{B}_e^{(1)T} \boldsymbol{F} \boldsymbol{B}_e^{(3)} \mathrm{d}A + \\ & \int_{A} \boldsymbol{G}_e^{(2)T} \boldsymbol{N} \boldsymbol{G}_e^{(2)} \mathrm{d}A - \int_{A} \boldsymbol{G}_e^{(2)T} \boldsymbol{N}^P \boldsymbol{G}_e^{(2)} \mathrm{d}A + \int_{A_e} \boldsymbol{B}_e^{(2)T} \boldsymbol{C}_s \boldsymbol{B}_e^{(2)} \mathrm{d}A + \int_{A_e} \kappa \boldsymbol{N}_e^{(2)T} \boldsymbol{N}_e^{(2)} \mathrm{d}A \Bigg)\end{aligned} \tag{2}$$

$$\boldsymbol{K}_{\mu} = \sum_{e=1}^{Ne} \mu \left(\int_{A_e} \kappa \boldsymbol{G}_e^{(2)T} \boldsymbol{G}_e^{(2)} \mathrm{d}A - \int_{A_e} \boldsymbol{L}_e^T \boldsymbol{N}_e^P \boldsymbol{G}_e^{(2)2} \mathrm{d}A + \int_{A_e} \boldsymbol{L}_e^T \boldsymbol{N}_e \boldsymbol{G}_e^{(2)2} \mathrm{d}A \right) \tag{3}$$

$$\boldsymbol{K}_{NL} = \sum_{e=1}^{Ne} \left(\int_{A_e} \frac{1}{2} \boldsymbol{B}_e^{(0)T} \boldsymbol{A} \boldsymbol{B}_{eNL}^{(0)} \mathrm{d}A + \int_{A_e} \boldsymbol{B}_{eNL}^{(0)T} \boldsymbol{A} \boldsymbol{B}_e^{(0)} \mathrm{d}A + \int_{A_e} \frac{1}{2} \boldsymbol{B}_{eNL}^{(0)T} \boldsymbol{A} \boldsymbol{B}_{eNL}^{(0)} \mathrm{d}A \right) \tag{4}$$

$$\boldsymbol{M} = \sum_{e=1}^{N_c} \left(\int_{A_c} I_0 \boldsymbol{N}_e^{(0)T} \boldsymbol{N}_e^{(0)} \mathrm{d}A + \int_{A_e} I_1 \boldsymbol{N}_e^{(1)T} \boldsymbol{N}_e^{(1)} \mathrm{d}A + \int_{A_e} I_0 \boldsymbol{N}_e^{(2)T} \boldsymbol{N}_e^{(2)} \mathrm{d}A \right) \tag{5}$$

and

$$\boldsymbol{M}_{\mu} = \sum_{e=1}^{N_c} \mu \left(\int_{A_e} I_0 \boldsymbol{G}_e^{(0)T} \boldsymbol{G}_e^{(0)} \mathrm{d}A + \int_{A_e} I_1 \boldsymbol{G}_e^{(1)T} \boldsymbol{G}_e^{(1)} \mathrm{d}A + \int_{A_e} I_0 \boldsymbol{G}_e^{(2)T} \boldsymbol{G}_e^{(2)} \mathrm{d}A \right) \tag{6}$$

where $\boldsymbol{B}_{eL}^{(0)}$, $\boldsymbol{B}_e^{(1)}$, $\boldsymbol{B}_e^{(2)}$, $\boldsymbol{N}_e^{(0)}$, $\boldsymbol{N}_e^{(1)}$, $\boldsymbol{N}_e^{(2)}$, $\boldsymbol{J}$, ∂_{ζ}, ∂_s, and J are explicitly shown in de Suarez and Rossi [17] while $I_i, i = 0, 1, 2$ are the mass inertia moments shown explicitly in Reddy [16]. Nanoscale coefficient μ and the Winkler foundation's elastic constant κ are used in these equations to introduce the scale consideration and the elastic medium, respectively. The displacement and rotation gradients are given by

$$\nabla(\boldsymbol{u})_e = \begin{bmatrix} u_{,x} & u_{,y} \\ v_{,x} & v_{,y} \end{bmatrix} \cong \boldsymbol{J} \partial_{\zeta} \boldsymbol{N}_{e(0)} \boldsymbol{U}_e, \boldsymbol{G}_e^{(0)} = \boldsymbol{J} \partial_{\zeta} \boldsymbol{N}_{e(0}, \tag{7}$$

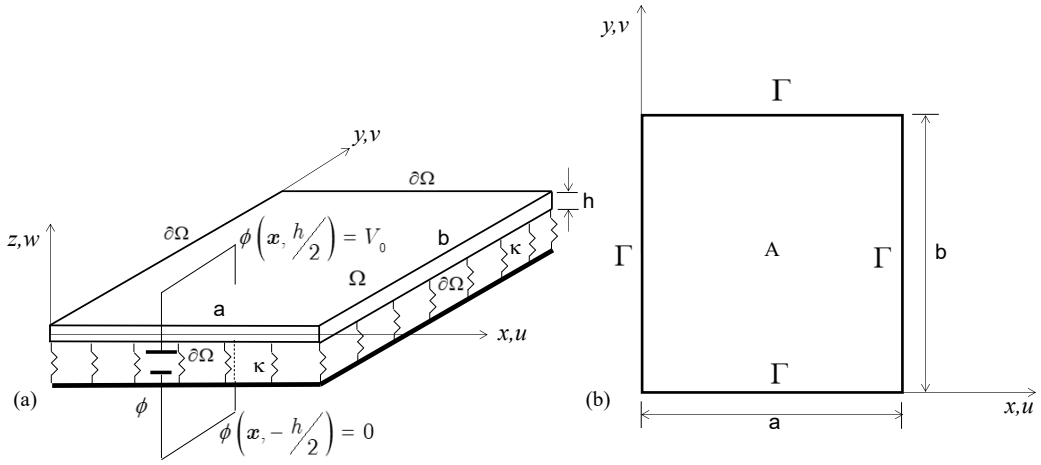

Figure 1. Plate model: a) Plate under elastic foundation and electric potential; b) dimensions of the middle plane of the plate.

$$\nabla\psi_e = \begin{bmatrix} \theta_{x,x} & \theta_{x,y} \\ \theta_{y,x} & \theta_{y,y} \end{bmatrix} \cong \boldsymbol{J}\partial_\zeta \boldsymbol{N}_{e(1)}\boldsymbol{U}_e, \boldsymbol{G}_e^{(1)} = \boldsymbol{J}\partial_\zeta \boldsymbol{N}_{e(1)}, \tag{8}$$

and

$$\nabla\left(w_0\right) = \begin{Bmatrix} w_{0,x} \\ w_{0,y} \end{Bmatrix} = \boldsymbol{G}_e^{(2)}\boldsymbol{U}_e, \quad \boldsymbol{G}_e^{(2)} = J^{-1}\partial_s \boldsymbol{N}_e^{(2)}. \tag{9}$$

The second order partial derivatives vector used in the formulation of the Laplacian and second order gradient are

$$\begin{Bmatrix} w_{,\xi\xi} \\ w_{,\xi\eta} \\ w_{,m} \end{Bmatrix} \cong \boldsymbol{G}_{e\zeta}^{(2)}\boldsymbol{U}_e = \partial_\zeta^2 \boldsymbol{N}_e^{(2)}\boldsymbol{U}_e, \boldsymbol{G}_{e\zeta}^{(2)} = \partial_\zeta^2 \boldsymbol{N}_e^{(2)}, \partial_\zeta^{2T} = \begin{Bmatrix} \frac{\partial(\cdot)}{\partial\xi^2} & \frac{\partial(\cdot)}{\partial\xi\partial\eta} & \frac{\partial(\cdot)}{\partial\eta^2} \end{Bmatrix} \tag{10}$$

and

$$\nabla\left(\nabla w_e\right) = \begin{Bmatrix} w_{,xx} \\ w_{,xy} \\ w_{,xy} \\ w_{,yy} \end{Bmatrix} \cong \boldsymbol{G}_e^{(2)2}\boldsymbol{U}_e, \boldsymbol{G}_e^{(2)2} = \boldsymbol{P}^{(0)}\left(\boldsymbol{J}^{-2}\boldsymbol{G}_{e\zeta}^{(2)2} - \boldsymbol{J}^{-2}\boldsymbol{J}_{x,2}\boldsymbol{J}^{-1}\boldsymbol{G}_{e\zeta}^{(2)}\right) \tag{11}$$

where $\boldsymbol{P}^{(k)}, k = 0, \ldots, 3$ are the following Boolean operators

$$\boldsymbol{P}^{(0)} = \begin{bmatrix} 1 & 0 & 0 \\ 0 & 1 & 0 \\ 0 & 1 & 0 \\ 0 & 0 & 1 \end{bmatrix}, \boldsymbol{P}^{(1)} = \begin{bmatrix} 1 & 0 & 1 \end{bmatrix}, \boldsymbol{P}^{(2)} = \begin{bmatrix} 1 & 0 \end{bmatrix}, \boldsymbol{P}^{(3)} = \begin{bmatrix} 0 & 1 \end{bmatrix}. \tag{12}$$

In Eq. 4, the nonlinear deformation and the Laplacian matrix are

$$\boldsymbol{\varepsilon}_{NL}^{(0)} \cong \frac{1}{2}\boldsymbol{B}_{NL}^{(0)}\boldsymbol{U}_c, \boldsymbol{B}_{NL}^{(0)} = \boldsymbol{A}_c^{(2)}\left(\boldsymbol{U}_c\right)\boldsymbol{G}_c^{(2)}, \boldsymbol{A}_c^{(2)}\left(\boldsymbol{U}_c\right) = \begin{bmatrix} \boldsymbol{P}^{(2)}\boldsymbol{G}_c^{(2)}\boldsymbol{U}_c & 0 \\ 0 & \boldsymbol{P}^{(3)}\boldsymbol{G}_c^{(2)}\boldsymbol{U}_c \\ \boldsymbol{P}^{(3)}\boldsymbol{G}_c^{(2)}\boldsymbol{U}_c & \boldsymbol{P}^{(2)}\boldsymbol{G}_c^{(2)}\boldsymbol{U}_c \end{bmatrix} \tag{13}$$

and

$$\nabla^2 (w_0) \cong \boldsymbol{L}_c^{(2)} \boldsymbol{U}_c, \boldsymbol{L}_c^{(2)} = \boldsymbol{P}^{(1)} \left(\boldsymbol{J}^{-2} \boldsymbol{G}_{c\zeta}^{(2)2} - \boldsymbol{J}^{-2} \boldsymbol{J}_{x,2} \boldsymbol{J}^{-1} \boldsymbol{G}_{c\zeta}^{(2)} \right) \tag{14}$$

where the operators $\boldsymbol{J}^{-2}, \boldsymbol{J}_{x,2}$ are explicitly shown in Zhang et al. [19]. The constitutive matrices $\boldsymbol{A}$, $\boldsymbol{C}_s$, $\boldsymbol{D}$, $\boldsymbol{F}$, and $\boldsymbol{E}$ are explicitly shown in Reddy [16], being $\boldsymbol{F}$ and $\boldsymbol{E}$ the piezoelectric constitutive matrices.

The internal normal force tensor and the piezoelectric normal force tensor are given by

$$\boldsymbol{N} = \begin{bmatrix} N_{xx} & N_{xy} \\ N_{xy} & N_{yy} \end{bmatrix}, \quad \boldsymbol{N}^P = h \begin{bmatrix} c_{31} V_0 & 0 \\ 0 & c_{31} V_0 \end{bmatrix} \tag{15}$$

The nonlinear eigenvalue/eigenvector problem shown in Eq. 1 is solved by the Interactive Progressive Method (IPM) in this work, as used in Sundararajan et al. [20]. However, in this work the effects of the internal forces are not considered in the update of the nonlinear stiffness matrix. Also, for this algorithm's operation it is necessary to establish the scale parameter w/h, that is a fixed relationship between the maximum transverse displacement and the height of the nanoplate section.

3 Numerical Results

The properties of the GFEM approximation space are now evaluated for the solution of the problem of free nonlinear vibrations, with two studies in mind: the comparative result relative to analytical and benchmark solutions, and the ability to capture the stiffness-softening and stiffness-hardening phenomena. Table 1 shows the main characteristics of each strategy used to solve the problem and will assist in making comparisons. Here the Winkler foundation's is not considered in the analysis.

Table 1. Numerica models.

Strategy	polinomial order	num element	NDOF
GFEM C^2	4	6x6 Q4	3675
FEM C^0	4	8x8 Q25	5053
Reference solution	biharmonic modes $(m = 20, n = 20)$	10x10 Q4	2000

3.1 Comparative Results

The comparative results are obtained considering the isotropic plate shown in Fig. 1 with aspect ratios $a/h = 1000$ and $a/b = 1$ and mechanics properties defined by Young modulus $E = 201.4 \times 10^9$ Pa, Poisson ratio $\nu = 0.28$, mass density $\rho = 8166$ kg/m^3, and shear correction coefficient $\kappa_S = 0.91$. The results for the strategies in Tab. 1 are presented in Fig. 2.

A. Result obtained by the analytical solution proposed by Chu and Herrmann [21];
B. Result obtained by FEM solution presented in Sundararajan et al. [20];
C. Result obtained by the Differential Quadrature Method (DQM) presented in Liu et al. [12];
D. Result corresponding to the GFEM C^2 strategy shown in Tab. 1.

In Fig. 2b the error is obtained relatively to the Chu and Herrmann [21] solution and calculated by

$$E_r = \frac{|\bar{\omega}_a - \bar{\omega}_h|}{|\bar{\omega}_a|} \times 100 \tag{16}$$

where $\bar{\omega}_h = (\omega_{NL}/\omega_L)_h$, $h = B, C$ and $\bar{\omega}_a = (\omega_{NL}/\omega_0)_a$, $a = A$. In Eq. 16 ω_{NL} and ω_L are the nonlinear and linear frequency, respectively. Also, ω_0 stands for the first analytical linear frequency obtained using Chu and Herrmann [21] approach.

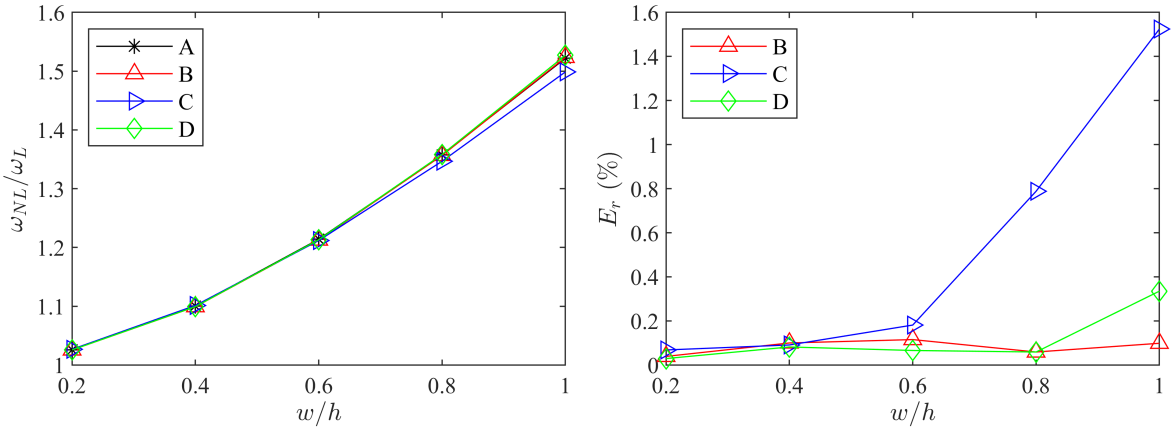

(a) Normalized frequency vs. normalized amplitude.

(b) Relative error (%) vs. normalized amplitude.

Figure 2. Graphical analysis of the comparative results.

Figure 2 shows the comparative results of strategies A-D. The poor result of the C strategy relatively to A solution, shown in Figs. 2a and 2b, occurs by the consideration of the normal forces in the C strategy. This consideration increases the stiffness of the plate and consequently an increase in the first natural frequency is expected.

3.2 Stiffness-softening and Stiffness-hardening phenomena

The stiffness-softening and stiffness-hardening phenomena are analyzed by the strategies proposed in Tab. 1 considering a simply supported piezoelectric nanoplate with ratios $a/h = 10$ and $a/b = 1$. This phenomenon is simulated by the increase of the nanoscale coefficient and the increase of the electric field intensity. The nanoplate is constituted of PZT-4, with physical properties shown in Tab. 1. The nanoplate is immersed in a transverse electric field, which is defined by

$$E_z(x, y, z, t) = -z\frac{e_{31}}{\kappa_{33}}\nabla \cdot \boldsymbol{\psi} + \frac{V_0}{h} \tag{17}$$

where $\boldsymbol{\psi}^T = \left\{ \begin{array}{cc} \theta_x & \theta_y \end{array} \right\}$ is the rotation vector, V_0 is the electric potential in the boundary $(x, y, h/2)$, $e_{ij}, i = 1, \ldots, 3, j = 1, \ldots, 6$ are de piezoelectric coefficients, and $\kappa_{ii}, i = 1, \ldots, 3$ the dielectric coefficients.

Table 2. Physical properties of PZT-4.

c_{11}(GPa)	c_{12}(GPa)	c_{13}(GPa)	c_{33}(GPa)	c_{44}(GPa)	c_{66}(GPa)
132	71	73	115	26	30.5
e_{13}(C/m^2)	e_{15}(C/m^2)	e_{13}(C/m^2)	κ_{11}(C/Vm)	κ_{22}(C/Vm)	κ_{33}(C/Vm)
-4.1	10.5	14.1	5.84×10^{-9}	5.84×10^{-9}	7.12×10^{-9}

Two cases of the scale effects on the first fundamental frequency are examined:

I Simulation of the stiffness-softening phenomenon produced by the increment of the nanoscale coefficient is shown in Fig. 3a. In this study, the effects of the transverse electric field are not considered.

II Simulation of the stiffness-hardening phenomenon, shown in Fig. 3b, is obtained for a piezoelectric nanoplate immersed in a transverse electric field, Eq. 17, through the increase of the positive electric potential in the top free surface of the nanoplate $(x, y, h/2)$ and for some values the nanoscale coefficient.

In these studies, the results are presented in terms of the normalized frequency

$$\bar{\omega} = a\omega\sqrt{\frac{I_0}{A_{11}}}. \tag{18}$$

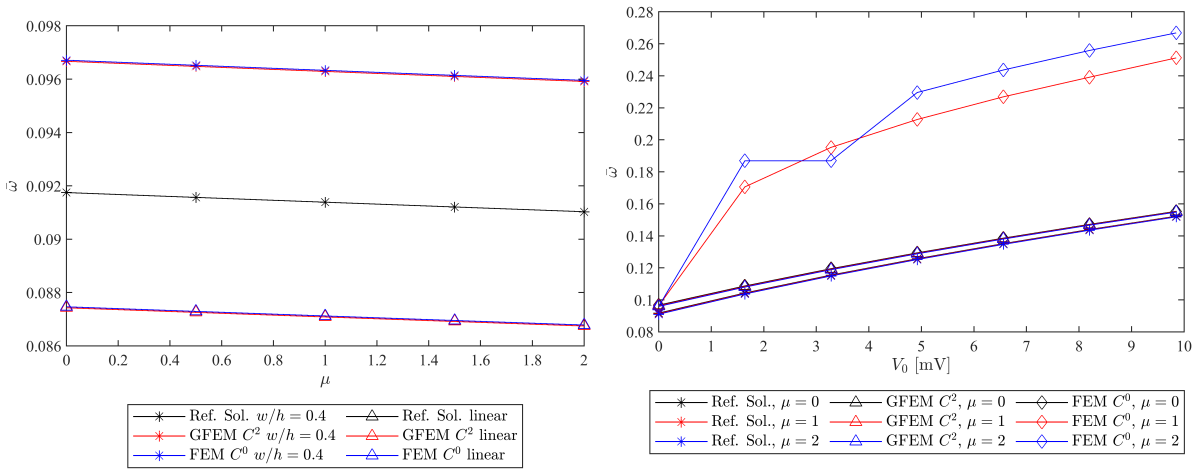

(a) Simulation of the stiffness-softening phenomenon.

(b) Simulation of the stiffness-hardening phenomenon for different values of V_0 and μ for $w/h = 0.4$.

Figure 3. Stiffness-softening and stiffness-hardening simulation.

The results shown in Fig. 3a demonstrate that the methodologies adopted adequately capture the stiffness-softening process. For the three numerical models in the present study, the linear response exhibits very similar behavior. However, when the nonlinear response is taken into account, the results demonstrate a considerable discrepancy between the Semi Analytical model and the models generated with GFEM C^2 and FEM C^0. Further analysis are been conducted to identify the source(s) for this deviation. Despite the small magnitude of the deviations, more studies are being conducted to identify and comprehend the source(s) of this deviation.

The results for stiffness-hardening phenomenon are shown in Fig. 3b. Notice that when the nanoscale coeddifient is taken into account the phenomenon is adequately described by the models derived from the GFEM C^2 and the semi-analytical solution, but not by the FEM C^0. This phenomena occurs because the second order partial derivatives in the discretized Laplacian (∇^2) and the second order gradient ($\nabla(\nabla w)$) in the FEM-Galerkin formulation cannot be accurately represented by the C^0 approximation spaces.

4 Conclusions

In this study, the Galerkin formulation adapted to non-local elasticity for an isotropic nanoplate of piezoelectric material was presented, considering the geometric non-linearity of von Karmann. The results obtained with GFEM C^2 and classical elasticity for the non-linear free vibration problem were close to those obtained in reference literature. The strategies used satisfactorily simulated the stiffness-softening phenomenon. On the other hand, the simulation of the stiffness-hardening phenomenon produced by the transverse electric field was satisfactorily represented only by the numerical models with high regularity approximation spaces. This study highlights the relevance of the regularity of approximation spaces in approaching certain types of problems. In this specific case, the model obtained with C^0 FEM-Lagrange is not able to satisfactorily approximate the effects of the Laplacians and the second-order gradients that appear in the Galerkin formulation of the problem.

Acknowledgements. The authors wish to acknowledge the support of CAPES, Coordenação de Aperfeiçoamento de Pessoal de Nível Superior, and also the CNPq, Conselho Nacional de Desenvolvimento Científico e Tecnológico of Brazil, grant number 309430/2021-6.

Authorship statement. This section is mandatory and should be positioned immediately before the References section. The text should be exactly as follows: The authors hereby confirm that they are the sole liable persons responsible for the authorship of this work, and that all material that has been herein included as part of the present paper is either the property (and authorship) of the authors, or has the permission of the owners to be included here.

References

[1] J. H. He, C. L. Hsin, J. Liu, L. J. Chen, and Z. L. Wang. Piezoelectric gated diode of a single zno nanowire. *Advanced Materials*, vol. 19, n. 6, pp. 781–784, 2007.
[2] Z. L. Wang. Zno nanowire and nanobelt platform for nanotechnology. *Materials Science and Engineering: R: Reports*, vol. 64, n. 3, pp. 33–71, 2009.
[3] U. Galan, Y. Lin, G. J. Ehlert, and H. A. Sodano. Effect of zno nanowire morphology on the interfacial strength of nanowire coated carbon fibers. *Composites Science and Technology*, vol. 71, n. 7, pp. 946–954, 2011.
[4] S. Xu and Z. L. Wang. One-dimensional zno nanostructures: Solution growth and functional properties. *Nano Research*, vol. 4, n. 11, pp. 1013–1098, 2011.
[5] M. Caglar, S. Ilican, Y. Caglar, and F. Yakuphanoglu. Electrical conductivity and optical properties of zno nanostructured thin film. *Applied Surface Science*, vol. 255, n. 8, pp. 4491–4496, 2009.
[6] Z. X. Huang, Z. A. Tang, J. Yu, and S. Bai. Thermal conductivity of nanoscale polycrystalline zno thin films. *Physica B: Condensed Matter*, vol. 406, n. 4, pp. 818–823, 2011.
[7] T. Belytschko, S. P. Xiao, G. C. Schatz, and R. S. Ruoff. Atomistic simulations of nanotube fracture. *Phys. Rev. B*, vol. 65, pp. 235430, 2002.
[8] S. Chowdhury and T. Okabe. Computer simulation of carbon nanotube pull-out from polymer by the molecular dynamics method. *Composites Part A: Applied Science and Manufacturing*, vol. 38, n. 3, pp. 747–754, 2007.
[9] A. E. Galashev and O. R. Rakhmanova. Molecular-dynamic calculation of effects appearing in removing a lead film from graphene. *Journal of Engineering Physics and Thermophysics*, vol. 90, n. 4, pp. 1026–1034, 2017.
[10] A. C. Eringen. Nonlocal polar elastic continua. *International Journal of Engineering Science*, vol. 10, n. 1, pp. 1–16, 1972.
[11] A. C. Eringen. On differential equations of nonlocal elasticity and solutions of screw dislocation and surface waves. *Journal of Applied Physics*, vol. 54, n. 9, pp. 4703–4710, 1983.
[12] C. Liu, L.-L. Ke, J. Yang, S. Kitipornchai, and Y.-S. Wang. Nonlinear vibration of piezoelectric nanoplates using nonlocal mindlin plate theory. *Mechanics of Advanced Materials and Structures*, vol. 25, n. 15-16, pp. 1252–1264, 2018.
[13] S. Zeng, B. Wang, and K. Wang. Nonlinear vibration of piezoelectric sandwich nanoplates with functionally graded porous core with consideration of flexoelectric effect. *Composite Structures*, vol. 207, pp. 340–351, 2019.
[14] S. R. Asemi, A. Farajpour, and M. Mohammadi. Nonlinear vibration analysis of piezoelectric nanoelectromechanical resonators based on nonlocal elasticity theory. *Composite Structures*, vol. 116, pp. 703–712, 2014.
[15] Z. Su, G. Jin, and T. Ye. Electro-mechanical vibration characteristics of functionally graded piezoelectric plates with general boundary conditions. *International Journal of Mechanical Sciences*, vol. 138-139, pp. 42–53, 2018.
[16] J. Reddy, ed. *Mechanics of Laminated Composite Plates and Shells Theory and Analysis*. CRC Press LLC, 2000.
[17] de O. A. G. Suarez and R. Rossi. A g/xfem approximation space based on the enrichment of rational polynomials to model free and forced vibration in elastic isotropic mindlin–reissner plates. *Journal of the Brazilian Society of Mechanical Sciences and Engineering*, vol. 41, n. 3, pp. 134, 2019.
[18] J. Sladek, V. Sladek, S. Hrcek, and E. Pan. The nonlocal and gradient theories for a large deformation of piezoelectric nanoplates. *Composite Structures*, vol. 172, pp. 119–129, 2017.
[19] L. Zhang, Y. Zhang, and K. Liew. Vibration analysis of quadrilateral graphene sheets subjected to an in-plane magnetic field based on nonlocal elasticity theory. *Composites Part B: Engineering*, vol. 118, pp. 96–103, 2017.
[20] N. Sundararajan, T. Prakash, and M. Ganapathi. Nonlinear free flexural vibrations of functionally graded rectangular and skew plates under thermal environments. *Finite Elements in Analysis and Design*, vol. 42, n. 2, pp. 152–168, 2005.
[21] H.-N. Chu and G. Herrmann. Influence of large amplitudes on free flexural vibrations of rectangular elastic plates. *Journal of Applied Mechanics*, vol. 23, n. 4, pp. 532–540, 2021.